Ionic conductivity and relaxations in $ZrO_2-Y_2O_3$ solid solutions

A. Pimenov[a],[*], J. Ullrich[a], P. Lunkenheimer[a], A. Loidl[a], C.H. Rüscher[b]

[a]*Experimentalphysik V, Universität Augsburg, D-86135 Augsburg, Germany*
[b]*Institut für Mineralogie, Universität Hannover, D-30167 Hannover, Germany*

1. Introduction

At high temperatures pure ZrO_2 reveals the cubic fluorite structure. This high-temperature phase can be stabilized in a solid solution of $ZrO_2-Y_2O_3$ below 1000°C. The resulting materials have found a wide area of application due to their high refractive index and stability against oxidation [1,2]. In addition, $ZrO_2-Y_2O_3$ was successfully used as substrate for high-T_c superconductors [3]. Even more importantly the stabilized ZrO_2 possesses a high ionic conductivity [4] of oxygen anions due to a large concentration of oxygen vacancies in the lattice. Oxygen vacancies are created by the trivalent yttria

atoms, used as dopants in the crystal structure. The oxygen conductivity opens the possibility to use $ZrO_2-Y_2O_3$ as solid electrolyte for high temperature fuel cells [5,6] and as sensitive element in oxygen sensors [7].

It is generally accepted [8], that the mobile oxygen ions are bound at temperatures below ~800 K and then gradually become mobile some hundred degrees above this temperature. As a result of this mechanism the measured dc conductivity shows a gradual change in slope in Arrhenius presentation from ~1.2 eV to ~0.8 eV [4,9,10]. Different microscopic models aiming to explain the observed temperature dependence of the effective activation energy are presented in the literature [11,12].

The frequency dependent conductivity of different yttria stabilized cubic zirconia single crystals was

[*]Corresponding author. Tel.: +49-821-598-3605; fax: +49-821-598-3649; e-mail: andrei.pimenov@physik.uni-augsburg.de

recently presented by Henn et al. [13]. In the frequency range 1 Hz–1 MHz the data were found to obey the following relation:

$$\sigma'(\omega) = \sigma_{dc} + A\omega^s. \qquad (1)$$

This relation is known as *universal dielectric response* (UDR) [14,15] and holds for a large variety of conducting materials. The analysis of the temperature dependence of the frequency exponent *s* gives the characteristic potential energy value $W_C = 0.29 \pm 0.05$ eV, which is in good agreement with the binding energy of the oxygen vacancies, obtained from the activation energy change of the dc conductivity [4,9,10].

We have investigated the frequency dependent conductivity of two commercially obtained yttria stabilized zirconia ceramics with molar concentrations 4 mol% and 8 mol% and of two ZrO_2–Y_2O_3 single crystals with yttria concentrations 10 mol% and 12 mol% in the frequency range 20 Hz–1 MHz and at temperatures 300–1100 K. In addition one representative sample (10 mol% crystal) was measured in the extended frequency range 5 Hz–1 GHz at room temperature.

2. Experimental details

In our measurements we used the ZrO_2–Y_2O_3 samples from different sources. The 4 mol% Y_2O_3 sample was a ceramic sensor material (oxygen sensor) from Bosch Co. The 8 mol% Y_2O_3 ceramics is obtained from Kerafol Co. The single crystals with 10 mol% and 12 mol% Y_2O_3 were grown from the melt under standard atmospheric conditions [16,17]. In the frequency range 20 Hz–1 MHz the measurements of the complex conductivity were performed using the HP4284 autobalance bridge. To make electrical contacts we covered the opposite planes of the sample with silver paint. The gold evaporated contacts, made for some measurements, yielded similar results. All experiments have been carried out in a high temperature furnace with the highest temperature being about 1100 K. For the 10 mol% Y_2O_3 sample the measurements were repeated in the frequency range 5 Hz to 10 MHz using a HP 4192A LF impedance analyzer. In the frequency range 1

MHz to 1 GHz a reflection technique using the HP4191 network analyzer was employed [18].

3. Results and discussion

Fig. 1 shows data for the ceramic sample with 4 mol% Y_2O_3 and for the single crystal with 10 mol% Y_2O_3. The results are plotted in the complex impedance plane Z″ vs. Z′. This type of presentation generally allows a clear separation of the different processes in ionically conducting samples [19]. Two semicircles and the onset of a third semicircle are observed in the spectra of the ceramic sample. With increasing impedance, we attribute these arcs to the bulk conductivity, the grain boundary and contact relaxation, as indicated in Fig. 1. The data on the single crystal are presented in the lower frame of Fig. 1. In contrast to the ceramic sample, only the arc of the intrinsic conductivity and the transition region to the contact relaxation can be seen. We used the complex impedance analysis for all samples investigated in order to separate the bulk dc conductivity from contact and grain boundary effects.

The frequency-dependent conductivities and the dielectric permittivities of the 4 mol% Y_2O_3
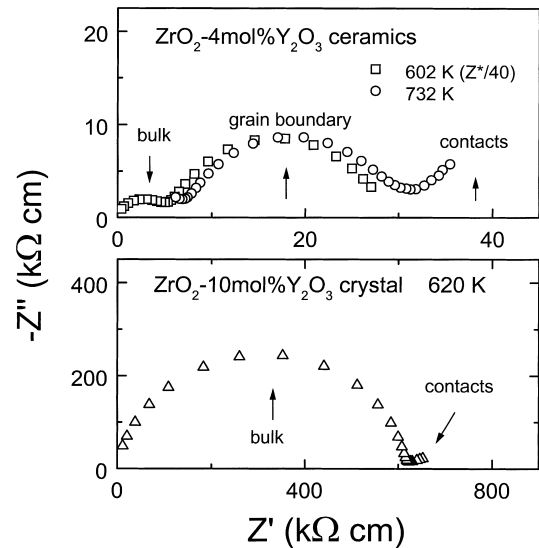

Fig. 1. Complex impedance presentation of ZrO_2–4 mol% Y_2O_3 ceramics and a ZrO_2–10 mol% Y_2O_3 single crystal. The arrows indicate different relaxations, as discussed in the text.
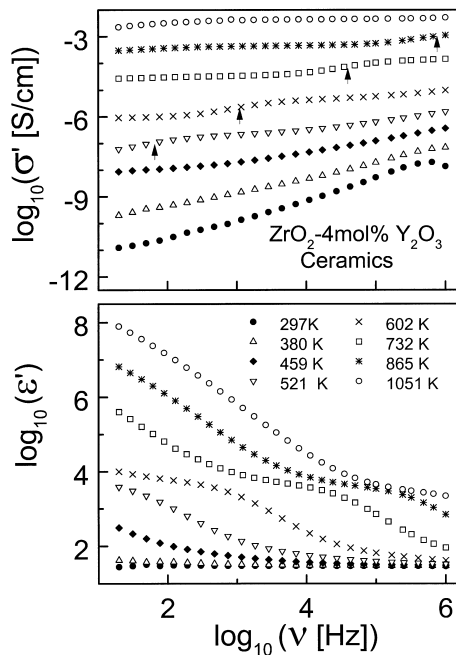
Fig. 2. Frequency dependent conductivity $\sigma'(\nu)$ (upper graph) and dielectric permittivity $\varepsilon'(\nu)$ (lower graph) of $ZrO_2 - 4$ mol% Y_2O_3 ceramics at different temperatures. The arrows indicate the positions of grain boundary relaxation.

ceramics are presented in Fig. 2. At room temperature ε' is nearly temperature independent and solely determined by its high frequency value $\varepsilon_\infty \approx 29$. With increasing temperature strong dispersion effects develop in $\varepsilon'(\nu)$. The dispersion steps shift to higher frequencies with increasing temperature and are accompanied by a step-like frequency dependence of $\sigma'(\nu)$ (upper frame). These smooth steps in $\sigma'(\nu)$ are to some extend masked due to the logarithmic format of the axes in Fig. 2 and their positions are marked by the arrows in the upper frame. We attribute these processes to the grain boundary relaxation in the sample [20] which is seen as a semicircle in the complex impedance plot of Fig. 1 and is not observed in the single crystals spectra (see also Ref. [4]). The grain boundary relaxation leads to the plateau of the dielectric permittivity of $\varepsilon'(\nu) \sim 10^4$ at intermediate frequencies and temperatures between 600 and 900 K.

At the three highest temperatures an additional increase of $\varepsilon'(\nu)$ with decreasing frequency is observed. This finding is quite usual for the complex

permittivity spectra of ionic conductors and can be ascribed to a blocking of the space charges near the electrodes [21]. The blocking electrodes affect the ac conductivity $\sigma'(\nu)$ at much lower frequencies as compared with the dielectric permittivity $\varepsilon'(\nu)$ but their influence still can be detected in the $\sigma'(\nu)$ curve at 1051 K as a decrease of the conductivity at frequencies below 100 Hz.

At low temperatures the dynamic conductivity σ' exhibits the typical signatures of an ionic conductor (Fig. 2). A power-law increase at high frequencies is preceded by the frequency independent plateau of dc conductivity. At higher temperatures the grain boundary effects modify this plateau and two different frequency independent plateaus of the conductivity on both sides of the grain-boundary relaxation (arrows in Fig. 2) can be observed. From the high frequency values the intrinsic conductivity of mobile ions can be extracted. The low frequency part reflects the properties of low-conducting regions between the grains.

The frequency dependence of the intrinsic part of the conductivity can be described by the UDR expression (Eq. (1)). But the frequency range of applicability of this expression is rather small due to the influence of the grain boundary relaxation and does not allow a reliable determination of parameters. An alternative way to present the data on ionic conductors is given by the modulus formalism [22] with $M^*(\nu) \equiv 1/\varepsilon^*(\nu)$. The modulus representation suppresses the unwanted effects of extrinsic relaxations and is often used in the analysis of dynamic conductivities of ionically conducting glasses. Although the physical meaning of this type of representation is still controversially discussed [23–25], the dielectric modulus is frequently used in the analysis of dielectric data of glassy ionic conductors [22,26,27]. The frequency ν_{max} of the peak, that shows up in $M''(\nu)$, is assumed to represent a characteristic frequency of the conductivity relaxation. If necessary, the correction factor in comparison with other presentations can always be calculated [28]. It is interesting to note, that for a large number of the experimentally observed spectra of ionically conducting materials, the frequency of the modulus peak lies in the transition region from dc to ac conductivity.

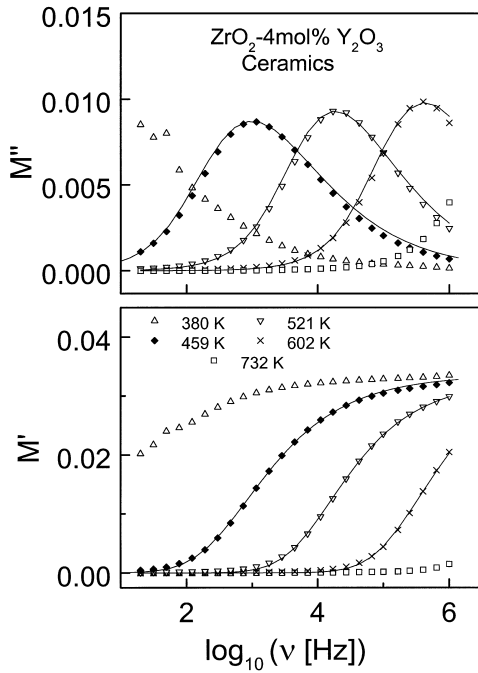Fig. 3 shows the results on $ZrO_2 - 4$ mol% Y_2O_3

Fig. 3. Frequency dependence of the real and imaginary part of the electric modulus M of ZrO_2–4 mol% Y_2O_3 ceramics at various temperatures. The solid lines are the results of least square fits using the Fourier transform of the KWW function (Eq. (2)) which have been performed simultaneously on $M'(\nu)$ and $M''(\nu)$.

ceramics as frequency dependent real and imaginary parts of the dielectric modulus. In order to analyze the data one can use the Fourier transform of the stretched exponential function:

$$\Phi(t) = \exp[-(t/\tau)^{\beta}]. \qquad (2)$$

The solid lines in Fig. 3 are the results of simultaneous fits of the real and imaginary parts of $M^*(\nu)$ according to Eq. (2). As can be clearly seen, the influence of grain boundaries and blocking electrode relaxations is effectively suppressed for the modulus data. The stretching exponent β can be estimated to be $\sim 0.5 \pm 0.05$ for the temperatures between 400 and 600 K, where reliable fits could be obtained. It should be noted, that the stretching parameter β is quite sensitive to the fit conditions and, consequently, the values are influenced by the small residual effect of the grain boundary relaxation. On the contrary, due to its large dynamic range and the

strong dependence upon temperature the conductivity relaxation time is not affected by the grain boundaries. The temperature dependence of the conductivity relaxation time is discussed below.

Fig. 4 shows the frequency dependence of the real parts of conductivity $\sigma'(\nu)$ (upper frame) and dielectric constant $\varepsilon'(\nu)$ (lower frame) of the ZrO_2–10% Y_2O_3 single crystal. For comparison, we show also the infrared data of Ref. [29], taken from the same single crystal using three different experimental techniques: quasi-optical complex transmission technique [30] at $6 \times 10^{10} < \nu < 10^{12}$ Hz, Kramers–Kronig analysis of reflectivity data at $10^{12} < \nu < 3 \times 10^{13}$ Hz and infrared transmission and reflectivity measurement at $3 \times 10^{13} < \nu < 10^{14}$ Hz.

At low frequencies a plateau characterizes the dc conductivity, and is followed by a power-law increase of the ac conductivity. The transition region from dc to ac conductivity shifts to higher frequencies with increasing temperature. In contrast to the data on the ceramics, only one plateau of the dc conductivity is observed. As it was demonstrated in Fig. 1, the grain boundary relaxation is no more
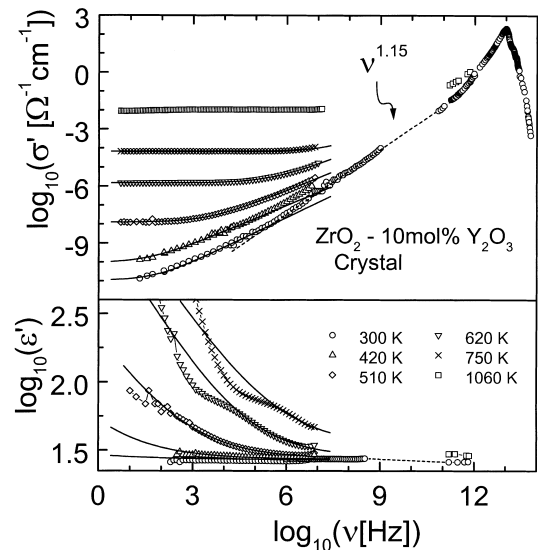

Fig. 4. Frequency dependent conductivity $\sigma'(\nu)$ (upper graph) and dielectric permittivity $\varepsilon'(\nu)$ (lower graph) of a ZrO_2–10 mol% Y_2O_3 single crystal at different temperatures. The relaxational process, seen on the $\varepsilon'(\nu)$ data corresponds to the bulk conductivity relaxation and lies in the transition region from dc to ac conductivity (upper graph).

present in the spectra and the contact effects are rather small and can hardly be observed on the logarithmic scale of Fig. 4. These peculiarities enable a closer inspection of the conductivity dispersion. For frequencies up to approximately three decades above the transition region the conductivity $\sigma'(\nu)$ can well be described using Eq. (1), as demonstrated by the solid lines in the upper frame of Fig. 4. The frequency exponent is determined as $s \approx 0.8$ near 300 K and then decreases with increasing temperature. This finding agrees with the analysis of ac conductivity in ZrO_2–Y_2O_3 single crystals, known from literature [13].

At high frequencies and low temperatures, $\sigma'(\nu)$ clearly deviates from the fits and shows a gradual increase of the local slope up to a value of about 1.15 at 10^8 Hz as indicated by the dashed line in Fig. 4. A slope approaching to or larger than one is often observed at high frequencies in glassy [31–33] as well as in crystalline ionic conductors [34,35]. At present there is no generally accepted explanation of this phenomena.

In the following we will discuss the dielectric permittivity $\varepsilon'(\nu)$ or, equivalently, the imaginary part of the complex conductivity $\sigma''(\nu) = 2\pi\nu\varepsilon_0\varepsilon'(\nu)$. The frequency dependence of ε' at various temperatures is shown in the lower part of Fig. 4. The data look qualitatively similar to those presented in Fig. 2: The dielectric permittivity decreases sharply at low frequencies due to contact effects, then indicates an intermediate plateau and, finally, levels off at highest frequencies at a value determined by ε_∞. A step-like increase is indicated at intermediate frequencies. The frequency of this step-like feature in the dielectric constant coincides with the transition frequency region from ac to dc conductivity. This is the main difference compared to the Fig. 2 of the ceramic sample where the characteristic frequencies of both effects differ by approximately 2–3 orders of magnitude. Thus the observed peculiarities of ε' as documented in Fig. 4 indicate the existence of an additional relaxation which has the intrinsic character. In the case of ceramic samples this relaxation could not be observed in the spectra because of the strong overlap of the bulk conductivity with the grain boundary relaxation. The observed frequency dependence of the dielectric permittivity can not be explained using only the universal dielectric response

in the form of Eq. (1), because the corresponding expression for the dielectric constant,

$$\epsilon'(\omega) = \varepsilon_\infty + A\omega^{s-1}\tan(s\pi/2)/\varepsilon_0, \qquad (3)$$

describes a monotonously decreasing function at low frequencies. This is demonstrated by the solid lines in the lower frame of the Fig. 4 which have been calculated using the Eq. (3) and the same parameters as obtained from the conductivity fits of the upper frame. Thus, some modifications of Eqs. (1) and (3) should be carried out at low frequencies or, alternatively, more complicated models [36–38] should be used to simultaneously describe the conductivity $\sigma'(\nu)$ and the dielectric constant $\varepsilon'(\nu)$.

We note, that according to the causality principle the real and imaginary parts of conductivity are not completely independent, but rather connected through the Kramers–Kronig (K–K) relations. Thus if a deviation from the K–K connected model in $\varepsilon'(\nu)$ is observed there should be similar effects in $\sigma'(\nu)$. Indeed, fine inspection of the transition region between ac and dc conductivities reveals some deviations, which, however, are too small to be seen in the logarithmic scale of Fig. 4.

A step-like character of $\varepsilon'(\nu)$ can well be described within the conductivity relaxation formalism, which was applied to the analysis of ionically conducting glasses by Howell et al. [39]. In this approach a step-like dielectric relaxation feature in ε' follows from simple considerations of a distribution of the conductivity relaxation times [22]. It should be noted, that within this approach there should always be a step-like frequency dependence of the dielectric permittivity, even for the data of ZrO_2–4% Y_2O_3 ceramics, shown in the lower part of Fig. 2, where due to the grain boundary effects it is not possible to decide, whether the $\varepsilon'(\nu)$ really saturates at low frequencies.

The 8 mol% ceramic sample and the 12 mol% single crystalline sample showed a qualitatively similar dielectric behaviour as the 4 mol% ceramic and the 10 mol% single crystalline sample respectively, only the absolute values being different. For all samples values of the dc conductivity have been extracted from the complex impedance plots and the values of the characteristic frequencies from the maximum of $M''(\nu)$. Having in mind the relaxation in

the frequency dependence of ε', we can now identify this frequency with the characteristic hopping frequency of dc conductivity. However, a correction factor possibly has to be introduced to determine the real mean conductivity relaxation rate.

Fig. 5 shows the dc conductivity and the modulus peak frequencies of the 4 mol% ceramic sample and 10 mol% single crystal as function of the inverse
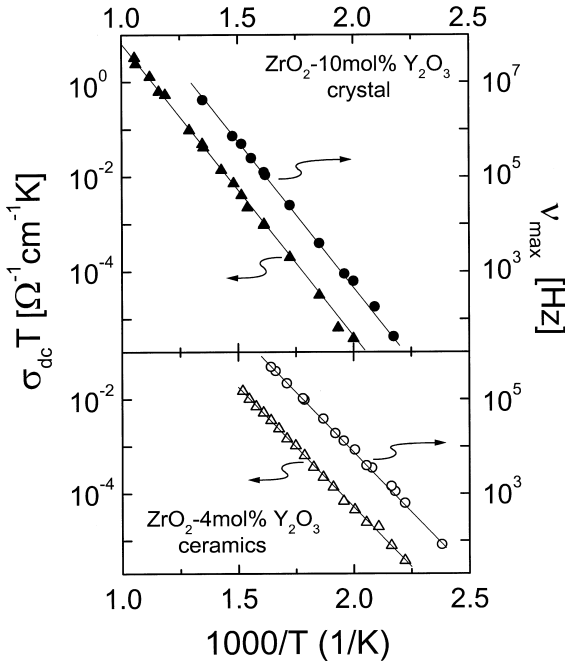

Fig. 5. Arrhenius plot of the dc conductivity and the peak frequency of the conductivity relaxation of ZrO_2–10 mol% Y_2O_3 single crystal and ZrO_2–4 mol% Y_2O_3 ceramics. The given values are extracted using the complex impedance (dc conductivity) and dielectric modulus (frequency of maximum $M''(\nu)$) presentations. The solid lines indicate the activation fits to the data with the *same* activation energy for conductivity and relaxation frequency.

temperature. Both properties are simply temperature activated in this temperature range and are proportional to each other. The solid lines indicate the fits to the data using the *same* activation energy for the dc conductivity and the mean relaxation frequency:

$$\sigma' \, T = A_0 \exp(-E_a/kT);$$
$$\nu_{max} = \nu_0 \exp(-E_a/kT). \tag{4}$$

The conductivity parameters of all samples investigated are summarized in Table 1. The 8 mol% ceramics has the maximal absolute value of conductivity in agreement with the observed conductivity maximum in this concentration range [8,40]. The activation energies are in agreement with the data given in literature for the low temperature region, where the vacancies are bound [8,9,11,40].

Finally, using the values of the dc conductivity and the characteristic frequency data, we can estimate the effective concentration of the mobile ions in the samples investigated. In this simple calculation we use the same procedure, based on the Nernst–Einstein relation as was applied to the $Zr_{0.85}Ca_{0.15}O_{1.85}$ single crystals by Orliukas et al. [41]. Assuming, that all carriers are free to migrate [42], one obtains:

$$\sigma_{dc} = \frac{nq^2 d^2 \gamma}{6} \frac{\omega_H}{kT} \tag{5}$$

where n and q are the carrier concentration and charge, d and ω_H are the characteristic hopping distance and frequency and γ is a geometrical factor. In the case of stabilized zirconia samples one can take for the product of geometrical factor and hopping distance [41,43]: $d^2\gamma = 0.35a^2$ with $a = 0.516$ nm being the structural parameter. The effec-

Table 1
Conductivity parameters of ZrO_2–Y_2O_3

Sample (mol% Y_2O_3)	$\sigma_{dc}(400°C)$ (Ω^{-1} cm^{-1})	ν_0 (s^{-1})	A_0 (Ω^{-1} cm^{-1}K)	E_a (eV)	n (cm^{-3})
4%	3.2×10^{-5}	1.1×10^{14}	7.4×10^5	1.01	9.4×10^{20}
8%	7.3×10^{-5}	5.4×10^{14}	3.5×10^6	1.05	9.0×10^{20}
10%	9.7×10^{-6}	1.0×10^{15}	9.6×10^6	1.22	1.3×10^{21}
12%	1.6×10^{-5}	2.0×10^{15}	1.3×10^7	1.22	9.0×10^{20}

The limiting high temperature values for the characteristic hopping frequency and the dc conductivity, ν_0 and A are extracted from the data using the *same* activation energy E_a (Eq. (4)). n is the effective mobile carrier concentration, estimated from Eq. (5).

tive carrier concentration, calculated for our samples using Eq. (5) are given in Table 1. These numbers are in good agreement with the concentration of the O^{2-} defects, introduced by doping [41].

4. Conclusions

We have investigated the electrical properties of $ZrO_2-Y_2O_3$ ceramics and single crystalline material of different molar concentrations from 4 mol% Y_2O_3 to 12 mol% Y_2O_3. The frequency dependent conductivities and dielectric constants were measured in the frequency range from 20 Hz to 1 GHz and for temperatures 300 K$\leq T \leq$1100 K. For the ceramic samples, two relaxations due to blocking electrodes and grain boundaries, are well documented in the spectra. The grain boundary relaxation is absent in the spectra of the single crystals. Using the complex impedance presentation from the measured spectra the absolute values of the bulk dc conductivity were extracted and compared with the published data. The frequency dependent conductivity can well be described using the universal dielectric response concept. In contrast, the dielectric constant reveals clear deviations from this approach. The main additional feature of the $\varepsilon'(\nu)$ spectra, observed for single crystals, is the well resolved relaxational 'step', corresponding to the transitional frequency region from dc to ac conductivity. The temperature dependence of the mean relaxation frequency is extracted from the maximum of the dielectric modulus peak. From our analysis we conclude, that the ac and dc conductivities in the $ZrO_2-Y_2O_3$ system are due to the same microscopical mechanism.

References

[1] V.I. Aleksandrov, V.F. Kitaeva, V.V. Osiko, N.N. Sobolev, V.M. Tatarintsev, I.L. Chistyi, Sov. Phys. Lebedev Inst. Rep. 3 (1975) 23.
[2] I.L. Chistyi, I.L. Fabelinskii, V.F. Kitaeva, V.V. Osiko, Y.V. Pisarevskii, I.M. Sil'vestrova, N.N. Sobolev, J. Raman Sp. 6 (1977) 183.
[3] B.P. Gorschunov, G.V. Kozlov, O.I. Sirotinskii, I.M. Chernyshev, Sov. Phys. Lebedev Inst. Rep. 2 (1989) 35.
[4] S.P.S. Badwal, J. Mater. Sci. 19 (1984) 1767.
[5] Y. Ohno, Y. Kaga, S. Nagata, Elect. Eng. Jpn. (USA) 107 (1987) 59.
[6] N.Q. Minh, J. Am. Ceram. Soc. 76 (1993) 563.
[7] W. Weppner, Solid State Ionics 52 (1992) 15.
[8] S.P.S. Badwal, Solid State Ionics 52 (1992) 23.
[9] F.T. Ciacchi, K.M. Crane, S.P.S. Badwal, Solid State Ionics 73 (1994) 49.
[10] S.P.S. Badwal, J. Am. Ceram. Soc. 73 (1990) 3718.
[11] J.D. Solier, I. Cachadiña, A. Dominguez-Rodriguez, Phys. Rev. B48 (1993) 3704.
[12] B.C.H. Steele, in: T. Takahashi (Ed.), High Conductivity Solid Ionic Conductors, Recent Trends and Applications, World Scientific, Singapore, 1989, p. 402.
[13] F.E.G. Henn, R.M. Buchanan, N. Jianng, D.A. Stevenson, Appl. Phys. A60 (1995) 515.
[14] A.K. Jonscher, Nature 267 (1977) 673.
[15] A.K. Jonscher, Dielectric Relaxation in Solids, Chelsea Dielectric Press, London, 1983.
[16] V.A. Aleksandrov, E.E. Lomonova, A.A. Maier, V.V. Osiko, V.M. Tatarintsev, V.T. Udovenchik, Kratkie Soobs. po Fizike 11 (1972) 3.
[17] H. Romer, K.-D. Luther, W. Assmus, Cryst. Res. Tech. 29 (1994) 787.
[18] R. Böhmer, M. Maglione, P. Lunkenheimer, A. Loidl, J. Appl. Phys. 65 (1989) 901.
[19] D. Ravaine, J.L. Souquet, in: P. Hagenmüller, W. Van Gool (Eds.), Solid Electrolytes, Academic Press, New York, 1978, p. 277.
[20] S.P.S. Badwal, Appl. Phys. A50 (1990) 449.
[21] J.R. Macdonald, W.B. Johnson, in: J.R. Macdonald (Ed.), Impedance Spectroscopy, Wiley, New York, 1987, p. 1.
[22] P.B. Macedo, C.T. Moynihan, R. Bose, Phys. Chem. Glasses 13 (1972) 171.
[23] C.T. Moynihan, J. Non-Cryst. Solids 172–174 (1994) 1395.
[24] S.R. Elliott, J. Non-Cryst. Solids 170 (1994) 97.
[25] D.L. Sidebottom, P.F. Green, R.K. Brow, J. Non-Cryst. Solids 183 (1995) 151.
[26] K.C. Sobha, K.J. Rao, Solid State Ionics 81 (1995) 145.
[27] J.M. Bobe, J.M. Reau, J. Senegas, M. Poulain, Solid State Ionics 82 (1995) 39.
[28] C.A. Angell, Chem. Rev. 90 (1990) 523.
[29] A. Pimenov, F. Kadlec, J. Petzelt, A.A. Volkov (to be published).
[30] A.A. Volkov, Y.G. Goncharov, G.V. Kozlov, S.P. Lebedev, A.M. Prochorov, Infrared Phys. 25 (1985) 369.
[31] R.H. Cole, E. Tombari, J. Non-Cryst. Solids 131–133 (1991) 969.
[32] C. Cramer, K. Funke, T. Saatkamp, D. Wilmer, M.D. Ingram, Z. Naturforsch. 50A (1995) 613.
[33] P. Lunkenheimer, A. Pimenov, A. Loidl, Phys. Rev. Lett. 78 (1997) 2995.
[34] A.A. Volkov, G.V. Kozlov, A.G. Pimenov, A.V. Sinitski, Ferroelectrics 126 (1992) 157.
[35] K. Funke, D. Wilmer, T. Lauxtermann, R. Holzgreve, S.M. Bennington, Solid State Ionics 86–88 (1996) 141.
[36] K. Funke, R. Hoppe, Solid State Ionics 40–41 (1990) 200.
[37] K. Funke, Philos. Mag. A68 (1993) 711.

[38] J.S. Dyre, J. Appl. Phys. 64 (1988) 2456.

[39] F.S. Howell, R.A. Bose, P.B. Macedo, C.T. Moynihan, J. Phys. Chem. 78 (1974) 631.

[40] G. Chiodelli, A. Magistris, M. Scarliotti, F. Parmigiani, J. Mater. Sci. 23 (1988) 1159.

[41] A. Orliukas, P. Bohac, K. Sasaki, L. Gauckler, J. Europ. Ceram. Soc. 12 (1993) 87.

[42] A.S. Nowick, W.-K. Lee, H. Jain, Solid State Ionics 28–30 (1988) 89.

[43] P. Abelard, J. Baumard, Phys. Rev. B26 (1982) 1005.